

Volumetric Exploitation of Synaptic Information using Context Localization and Evaluation

William Gray Roncal, Verena Kaynig-Fittkau, Narayanan Kasthuri,
Daniel Berger, Joshua T. Vogelstein, Lindsey R. Fernandez, Jeff W Lichtman,
R. Jacob Vogelstein, Hanspeter Pfister, Gregory D. Hager

Johns Hopkins University, Massachusetts Institute of Technology, Harvard University

Abstract. In the emerging field of connectomics, researchers work to elucidate the wiring diagram of the brain; one goal is to complete a mapping at an ultrastructure resolution (i.e., each neuron and its synaptic connections). Although much progress has been made in recent years, additional work is needed to develop a fully automated system to reliably find all graph vertices, edges, and their attributes. This paper presents a novel method for synapse detection using bouton localization and biological context, in a multistage semantic segmentation approach. Our approach is comparable to state-of-the-art performance while demonstrating significant savings in computation and improvements in scalability.

Keywords: electron microscopy, synapse detection, image processing, segmentation, grammar, connectomics

1 Introduction

Mammalian brains are composed of millions to billions of neurons, and orders of magnitude more interconnections (i.e., synapses) [1]. To date, the full reconstruction of the neuronal connections of an organism, a “connectome,” has only been completed for nematodes with hundreds of neurons and thousands of synapses [2,3]. It is generally accepted [4,5] that such wiring diagrams are useful for understanding brain function and contributing to medical advances. For example, many psychiatric illnesses, including autism and schizophrenia, are thought to be “connectopathies,” where inappropriate wiring mediates pathological behavior [6,7]. Due to the problem scale, automatic segmentation of a neuronal network, consisting of tracing neural processes (i.e., graph nodes) and identifying the connections between them (i.e., graph edges) is required.

Although a complete solution is still elusive, researchers have made great progress towards automatically and comprehensively tracking all neurites through dense electron microscopy data [8,9,10,11]. However, current state-of-the-art methods for finding synaptic edges are still incomplete and insufficient, especially for large-scale automated circuit reconstruction.

Previous methods have taken several approaches, including manual segmentation, identification of post-synaptic densities (PSDs), filtering PSDs with vesicle information, and restricting a synapse search to membrane boundaries in

proximity to vesicle fields [11,12]. Two recent approaches [13,14] address the synapse detection problem in post-stained, isotropic, focused ion beam scanning electron microscopy (FIBSEM) data. The former uses a Random Forest voxel-based classifier and texture-based features to leverage identification of the pronounced post-stained post-synaptic densities. This approach is insufficient for our application because of the anisotropy and much lower contrast of our synaptic regions, as well as the computational expense. The latter approach also uses a voxel-based classification approach and features similar to [13]. However, [14] extends the approach by considering biological context by extracting information from surrounding pre- and post-synaptic regions at various sizes and locations, based on the synapse pose. This technique relies on full 3D contextual information and greatly reduces false positives from [13].

Our approach builds on many of these ideas and extends them by considering additional context information (e.g. bouton locations), and segmentation labels. This algorithm has been tested on publicly available, non post-stained anisotropic cortical data acquired with serial section transmission electron microscopy. The largest datasets currently available (and of sufficient size to begin estimating graphs) are acquired using scanning electron microscopy (SEM) and transmission electron microscopy (TEM) methods due to their high throughput capability [15,16]. This methodology scales well, but produces thick, anisotropic slices relative to in-plane resolution (a limitation of the method), and often does not have optimal staining to enhance synaptic contacts (due to throughput considerations and the potential for introducing noise). Our classifier is robust to

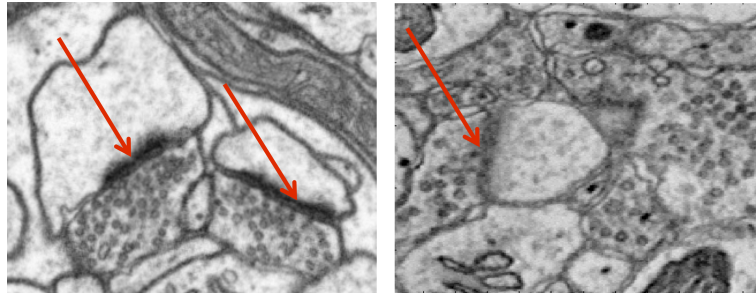


Fig. 1: Synapses in isotropic post-stained volume (left), and anisotropic non post-stained volume (right). Only objects indicated by the red arrows are synaptic junctions. Isotropic data courtesy of Graham Knott, <http://www.incf.org/about/who-we-are/nodes/switzerland/data>

these challenges, and can be straightforwardly extended to isotropic or stained data. Our result was directly compared to the method in [14] (which was found to be superior to [13]). Our result demonstrated comparable performance with a substantial savings of computational cost; moreover, in addition to performing segmentation, our approaches assigns a semantic annotation to each voxel, obviating the need for an additional layer of complexity towards our goal of circuit inference.

2 Method

The goal of this research is to produce a scalable, adaptive method for axo-dendritic synapses. We take a multistage, multiscale approach, each subsequent stage operating at a coarser scale, typical of a fine-to-coarse strategy. In the first stage, we apply a classifier to all voxels in the volume yielding a *membrane* or *segment* label. Each segment is fully enclosed by membranes, and each membrane contains only a single segment (modulo errors). Each segment consists of all the voxels within a two-dimensional closed contour. Although tools are readily available for implementing such a pre-processing step [8,9,10], we utilize manual segmentations to demonstrate our method. We call each membrane or segment a *two-dimensional (2D) object*. Note that some membranes will become putative synapses and some segments will become putative boutons.

In the second state, we classify 2D segments into *bouton* or *not bouton* (see Section 2.1). In the third stage, we fuse 2D membranes and classify 3D membranes as *synapse* or *not*. These latter two stages bring serious statistical challenges. Most theoretical and methodological work in statistics has focused on classifying finite dimensional Euclidean objects. However, our objects do not natively live in such a space (as described below).

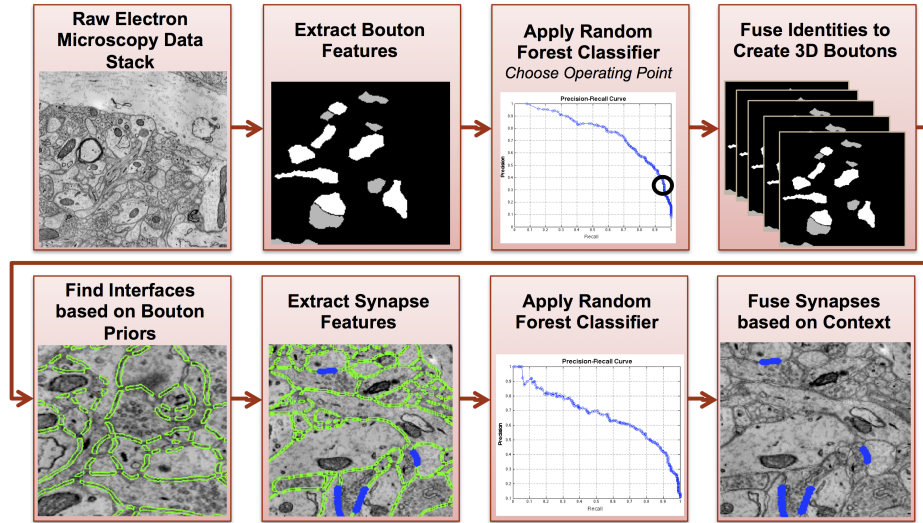


Fig. 2: Illustration of overall approach presented in this manuscript: bouton localization, followed by synapse classification and fusion.

2.1 Bouton Detection

The synapses of interest occur along cell membrane boundaries, between (at least) two neural processes. The pre-synaptic side is known as a bouton, characterized by a bulbous end filled with small vesicles. Each bouton can have a

complicated three-dimensional (3D) shape, size, and texture. Thus, each object can be represented by a 4D surface: three spatial dimensions and a fourth intensity dimension (encoding texture, for example). We desire to build a classifier on such 4D surfaces.

Formally, we have the following setting. We observe $\{(x_i, y_i)\}_{i \in [n]}$, where each $x_i \in \mathcal{X}$ is an element of the space of 4D objects to classify, and each $y_i \in \mathcal{Y}$ is an element of the space of possible labels (bouton or not), and $[n] = \{1, \dots, n\}$. Our goal is to train a classifier, $\hat{g}_n(\cdot): \mathcal{X} \times (\mathcal{X} \times \mathcal{Y})^n \rightarrow \mathcal{Y}$, that utilizes a training corpus of size n to make the best possible label prediction on a novel test data point, x . Our criterion of optimality is governed by the downstream inference task of connectome inference. This is in contrast to previous work, which assesses performance based on voxel-centric metrics [13,14].

We embed each slice of the surface into finite dimensional Euclidean space via constructing a set of functionals that operate on the slice; instead, we consider each 2D slice of the three spatial dimensions independently. Our features are all functionals of the 4D surface; some operate only on the 1D, 2D, or 3D marginals—a summary of our feature set appears in Table 1; features are generated by computing mean, median, entropy and variance over the applicable regions.

Feature Name	Step Used
size (number of voxels in object; voxels above/below threshold)	BY
region properties (eccentricity and solidity)	Y
bouton score of adjacent objects (difference, raw scores, intensity, size)	Y
entropy (neighborhood and region)	BY
intensity (mean, median, min/max, number above/below threshold)	BY
histogram measurements	B
gradient information (histogram of oriented gradients, magnitude)	BY
Laplacian of Gaussian	BY
Hough transform (circle case)	B
structure tensor eigenvalues	BY
hessian eigenvalues	BY
local binary patterns	BY

Table 1: Description of features used in method; in step used column, B indicates bouton step and Y indicates synapse step

Let ϕ be the set of functionals operating on the slices resulting in the above features. Given ψ , we can train many standard classifiers, $\hat{g}_\psi: \psi(\mathcal{X}) \times (\psi(\mathcal{X}) \times \mathcal{Y})^n \rightarrow \mathcal{Y}$, where $\psi(\mathcal{X}) = \{\eta: \psi(x) = \eta \forall x \in \mathcal{X}\}$. We opted for a random forest classifier [17] due to its robust finite sample performance in relatively high-dimensional and nonlinear settings, such as ours. The output of the random forest is a scalar, which we threshold to obtain a class label. The threshold is chosen to be high to avoid having many false negatives (false positives can be discarded via other means). Finally, we fuse these 2D boutons with the 2D boutons in the adjacent slices, whenever the number of overlapping voxels exceeds some threshold, yielding 3D boutons.

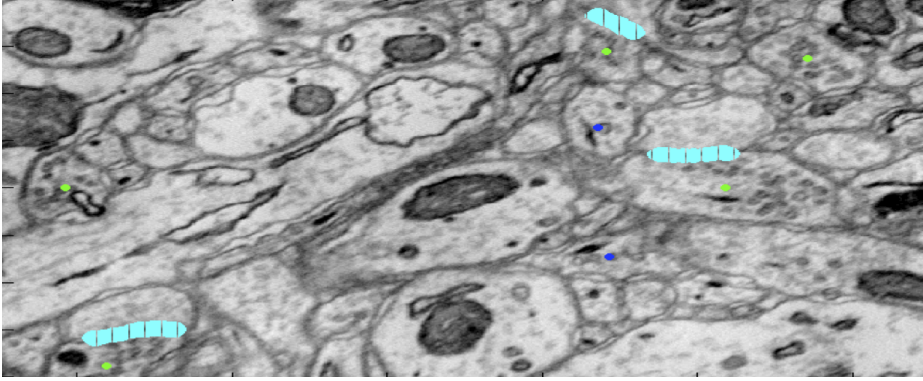


Fig. 3: Bouton Detection Results Over Slice of Image Volume

2.2 Synapse Detection

The above procedure yields a number of 2D bouton slices and non-boutons. Because, by definition each synapse is associated with a bouton, we can now search for synapses based on our 2D bouton classifier outputs. Specifically, we dilate each 2D bouton, and find connected objects. The overlapping voxels that are also members of the membrane label class become z_i , the 2D putative synapse slices that we hope to classify. Moreover, adjacent to each z_i are other segments; call the collection of all such 2D segments v_i . Now, we would like to build a classifier, $\hat{h}_n: \mathcal{Z} \times \mathcal{V} \times (\mathcal{Z} \times \mathcal{V} \times \mathcal{J})^n \rightarrow \mathcal{Y}$, where \mathcal{Z} and \mathcal{V} correspond to the space of z_i 's and v_i 's, respectively.

As in the above setting, learning such a classifier in the native space is daunting. Therefore, we again define functions $\psi_z: \mathcal{Z} \rightarrow \mathbb{R}^{d_z}$ and $\psi_v: \mathcal{V} \rightarrow \mathbb{R}^{d_v}$. Given these functions (which look quite similar to their ψ counterpart), we can again apply standard techniques like a random forest classifier. Note that because we are only classifying the z_i 's, and not the v_i 's, this problem is reminiscent of other transfer and semi-supervised learning settings. Also note that the random forest classifier outputs a scalar value, called a score, that can be thresholded as desired.

The above gives us a collection of 2D putative synapse slices. We are interested, however, in finding the full 3D spatial extent of each synapse. Putative synapse candidates are thus fused into 3D objects using a similar strategy as employed above. Eliminating all 3D putative synapses whose average 2D putative synapse slice score is less than β of the maximum average putative synapse score for that bouton. This pruning step eliminates a large number of false positives with little impact to recall. Then we assign a final score to each putative synapse, using the heuristic below; the first part of the function captures the idea that synapses should persist across multiple slices, and the second part emphasizes the importance of a strong response on at least one slice.

Let \mathcal{J}_i indicate the set of all the 2D putative synapses associated with a 3D putative synapse, and let s_j indicate the score of 2D putative synapse review. We define:

$$S_i := \alpha \cdot \left(\sum_{j \in \mathcal{J}_i} \mathbb{I}\{s_j > t\} \right) + (1 - \alpha) \cdot \left(\max_{\forall i} s_i \right), \alpha \in [0, 1], t \in (0, \infty).$$

We generate a precision-recall curve by sweeping across a threshold as before, and detection rates are computed at each point. If detailed synaptic morphology is required, a region-growing algorithm may be applied, using these locations as seed points.

3 Evaluation

The algorithm presented in this paper was evaluated on an anisotropic ($6 \times 6 \times 30nm$ resolution) data set of non post-stained mouse cortex as described in [16]. This data is extracted from a much larger EM volume ($\sim 100 \times 100 \times 50 \mu m^3$), and is part of the region known in the community as AC3. 90 slices ($\sim 6 \times 6 \times 2.7 \mu m^3$) were used for training, and an additional 50 slices ($\sim 6 \times 6 \times 1.5 \mu m^3$, non-contiguous with the training data) were used as a closed validation dataset.

3.1 Scalability

This work enables large-scale processing because of its light computational footprint and ability to be easily parallelized in a cluster setting. Relative to comparison methods [14], it can be run approximately twice as fast (even using unoptimized MATLAB code) on a laptop (versus a workstation) with an order of magnitude less RAM (10 GB versus more than 100 GB). Our method of synaptic edge detection is fully compatible with the Open Connectome Project’s LONI-based connectomics estimation pipeline, and the results presented in this paper will be integrated into the Open Connectome Project, and available at <http://www.openconnectome.org/catmaid>.

3.2 Performance

Truth labels for synapses were completed by an expert annotator, and bouton labels were completed independently by a skilled annotator outside the evaluation and training process. The training labels were visually inspected for consistency; however, our results were completed as an open-loop process, and not fed back to assess truthing accuracy.

The method in [14] was evaluated by up-sampling our data and label slice to approximately isotropic ($6 \times 6 \times 6nm$ resolution). 300 isotropic slices were used for training (corresponding to 60 of our original slices), and the result was computed on the full isotropic test set. In order to compute detection metrics, the raw responses were thresholded at different operating points, and clusters surviving a minimum size criteria were labeled a putative 3D synapse. This

process was only possible at high threshold values, so that each synaptic cluster represented only one distinct object. We evaluated performance using manually labeled two-dimensional membrane segments as a preprocessing step.

As discussed in the introduction, we are interested in finding synapses as a detection problem, and so precision-recall is used instead of voxel error metrics. The precision recall curves shown below demonstrate that we can correctly label boutons in our data, and use this information to locate synapses with performance comparable to that of [14].

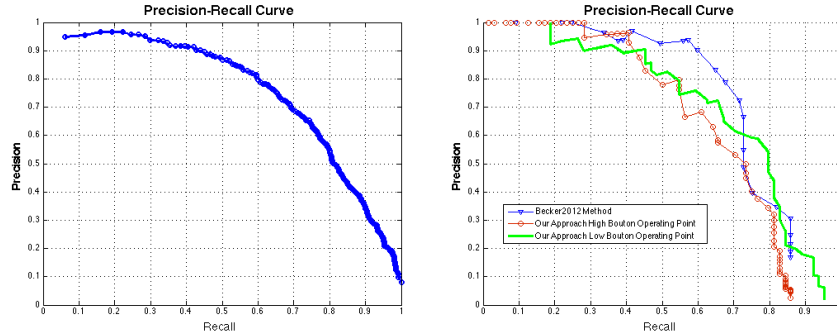


Fig. 4: Results for 2D Bouton detection (left), and 3D Synapse detection (right).

4 Conclusion

In this paper we have presented an efficient synapse detector that works on non post-stained, anisotropic EM data, and have shown it has comparable performance to methods requiring significantly more computation and memory. It addresses the problem of synapse detection in a manner consistent with that of expert human annotators, and is implemented in a manner that is robust, scalable and easily applied to large, real-world datasets. We implement a semantic segmentation framework for bouton and synapse detection that emphasizes the presence or absence of a connection between two neural processes, and provides a straightforward approach for assessment.

References

1. G M Shepherd. *The Synaptic Organization of the Brain*. Oxford University Press, USA, 2004.
2. J. G. White, E. Southgate, J. N. Thomson, and S. Brenner. The Structure of the Nervous System of the Nematode *Caenorhabditis elegans*. *Philosophical Transactions of the Royal Society B: Biological Sciences*, 314(1165):1–340, 1986.
3. Daniel J Bumbarger, Metta Riebesell, Christian Rödelsperger, and Ralf J Sommer. System-wide Rewiring Underlies Behavioral Differences in Predatory and Bacterial-Feeding Nematodes. *Cell*, 152(1-2):109–19, 2013.

4. Jeff W Lichtman and Winfried Denk. The big and the small: challenges of imaging the brain's circuits. *Science (New York, N.Y.)*, 334(6056):618–23, 2011.
5. Olaf Sporns, Giulio Tononi, and R. Kötter. The human connectome: a structural description of the human brain. *PLoS Computational Biology*, 1(4):e42, 2005.
6. Jennifer Fitzsimmons, Marek Kubicki, and Martha E Shenton. Review of functional and anatomical brain connectivity findings in schizophrenia. *Current opinion in psychiatry*, 26(2):172–87, 2013.
7. Graeme Martin. Network analysis and the connectopathies: current research and future approaches. *Nonlinear dynamics, psychology, and life sciences*, 16(1):79–90, 2012.
8. Amelio Vazquez-Reina, Michael Gelbart, Daniel Huang, Jeff Lichtman, Eric Miller, and Hanspeter Pfister. Segmentation fusion for connectomics. *2011 International Conference on Computer Vision*, pages 177–184, 2011.
9. J. Funke, B. Andres, F. a. Hamprecht, A. Cardona, and M. Cook. Efficient automatic 3D-reconstruction of branching neurons from EM data. In *Conference on Computer Vision and Pattern Recognition*, pages 1004–1011. IEEE, 2012.
10. Verena Kaynig-Fittkau. *Machine Learning Approaches for Neuron Geometry Extraction and Synapse Detection in Electron Microscopy Images*. PhD thesis, ETH Zurich, 2011.
11. Yuriy Mishchenko, Tao Hu, Josef Spacek, John Mendenhall, Kristen M Harris, and Dmitri B Chklovskii. Ultrastructural Analysis of Hippocampal Neuropil from the Connectomics Perspective. *Neuron*, 67(6):1009–1020, 2010.
12. Angel Merchán-Pérez, José-Rodrigo Rodríguez, Lidia Alonso-Nanclares, Andreas Schertel, and Javier Defelipe. Counting Synapses Using FIB/SEM Microscopy: A True Revolution for Ultrastructural Volume Reconstruction. *Frontiers in Neuroanatomy*, 3:18, 2009.
13. Anna Kreshuk, Christoph N Straehle, Christoph Sommer, Ullrich Koethe, Marco Cantoni, Graham Knott, and Fred a Hamprecht. Automated detection and segmentation of synaptic contacts in nearly isotropic serial electron microscopy images. *PloS One*, 6(10):e24899, 2011.
14. Carlos Becker, Karim Ali, Graham Knott, and Pascal Fua. Learning Context Cues for Synapse Segmentation in EM Volumes. *Medical Image Computing and Computer Assisted Intervention*, 7510:585–592, 2012.
15. Davi D Bock, Wei-chung Allen Lee, Aaron M Kerlin, Mark L Andermann, Greg Hood, Arthur W Wetzel, Sergey Yurgenson, Edward R Soucy, Hyon Suk Kim, and R Clay Reid. Network anatomy and in vivo physiology of visual cortical neurons. *Nature*, 471(7337):177–182, 2011.
16. Narayanan Kasthuri, Ken Hayworth, Juan C Tapia, Richard Schalek, S Nundy, and Jeff W Lichtman. The brain on tape: Imaging an Ultra-Thin Section Library (UTSL). *Society for Neuroscience Abstract*, 2009.
17. Leo Breiman. Random forests. *Machine learning*, pages 5–32, 2001.

Acknowledgements: Thanks to Dean M. Kleissas, H. Sebastian Seung, and Ayushi Sinha for technical discussions and advice and to Randal M. Burns and Priya Manavalan for providing the Open Connectome Project infrastructure.